BIOCHEMISTRY
including biophysical chemistry & molecular biology

Article

pubs.acs.org/biochemistry

Computational Studies of the Cholesterol Transport between NPC2 and the N-Terminal Domain of NPC1 (NPC1(NTD))

Guillermina Estiu,[†] Nazir Khatri,[†,‡] and Olaf Wiest*[,†,§]

[†]Department of Chemistry and Biochemistry and the Center for Rare and Neglected Diseases, University of Notre Dame, Notre Dame, Indiana 46556, United States

[‡]Department of Chemistry, Franklin College, Franklin, Indiana 46131, United States

[§]The Lab of Computational Chemistry and Drug Design, Laboratory of Chemical Genomics, Peking University Shenzhen Graduate School, Shenzhen 518055, P.R. China

Supporting Information

ABSTRACT: The transport of cholesterol from NPC2 to NPC1 is essential for the maintenance of cholesterol homeostasis in late endosomes. On the basis of a rigid docking model of the crystal structures of the N-terminal cholesterol binding domain of NPC1-(NTD) and the soluble NPC2 protein, models of the NPC1(NTD)-NPC2-cholesterol complexes at the beginning and the end of the transport as well as the unligated NPC1(NTD)-NPC2 complex were studied using 86 ns MD simulations. Significant differences in the cholesterol binding mode and the overall structure of the two proteins compared to the crystal structures of the cholesterol binding separate units were obtained. Relevant residues for the binding are identified using MM/GBSA calculations and the influence of the mutations analyzed by modeling them *in silico*, rationalizing the results of previous mutagenesis experiments. From the calculated energies and the NEB (nudged elastic band) evaluation of the cholesterol transfer mechanism, an atomistic model is proposed of the transfer of cholesterol from NPC2 to NPC1(NTD) through the formation of an intermediate NPC1(NTD)-NPC2 complex.

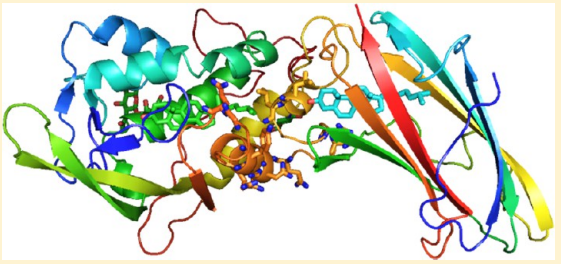

The maintenance of proper cholesterol homeostasis and metabolism is essential for cellular function. The pioneering work of Brown and Goldstein elucidated the tightly controlled receptor mediated pathway for cholesterol homeostasis.[1,2] More recently, much attention was focused on the removal of cholesterol, formed by hydrolysis of cholesterol esters by lysosomal acid lipase (LAL), from the endosomes/lysosomes (LE) to the ER. This process is thought to be mediated by two proteins, NPC1 and NPC2, which were found to be essential for cholesterol homeostasis.[3−6] NPC2 is a soluble, 132 residue protein that binds cholesterol with high affinity,[7,8] while NPC1 is a large, 1278 residue membrane-bound protein.[9] The crystal structures of full-length NPC2 with and without cholesterol are known (pdb IDs 2HKA and 1NEP).[7] Because of the complexity of NPC1, only the cholesterol binding domain of NPC1 containing the ∼240 N-terminal residues, the so-called NPC1(NTD), has been expressed, and its structure was determined by X-ray crystallography with and without cholesterol bound.[10,11] The protein−protein complex of NPC1 and NPC2 has not been directly observed, presumably due to its low association constant, and its structure is not known. Thus, there are many unanswered questions with respect to the unknown protein−protein complex and the precise mechanism of the involvement of these two proteins in cholesterol efflux from the LE, making it a topic of intense ongoing work.[3−5,10,12−16]

In order to explain the NPC1−NPC2 dual dependence of cholesterol transport, a model was proposed that postulates an interaction of NPC2 with NPC1, allowing cholesterol to slide from NPC2 to NPC1 without having to enter the water phase.[10] This so-called sliding model is supported by X-ray crystallography, showing the opposite orientation of cholesterol in the two binding sites and by alanine scanning mutagenesis. The latter has localized "patches" on the surface of both proteins that are not required for cholesterol binding but are required for cholesterol transfer from NPC2 to NPC1. The most important mutations defining the patches, which transferred less than 25% of bound cholesterol to liposomes, replaced residues L175/L176, D180/D182, N185, T187/N188, E191/Y192, and G199/Q200, located in a subdomain of NPC1(NTD) spanning amino acids in helices 7 and 8 and the intervening loop. Of the six mutants in this region, the two most deficient in transfer are L175A/L176A and E191A/Y192A. In modeling studies, these patches could be aligned so as to bring the two cholesterol binding sites into close proximity, in such a way that the plane of the cholesterol would be held constant as the sterol slides from NPC2 to NPC1.[10,14] The mutagenesis studies demonstrated that NPC1 and NPC2 function as the cellular "tag team duo" to catalyze the

Received: May 1, 2013
Revised: August 27, 2013
Published: September 3, 2013

mobilization of cholesterol but do not prove uniquely the direction of cholesterol trafficking. In the model, this directionality is hypothesized in order to better explain the entrance of cholesterol to the lysosomal membrane when its hydrophobic isooctyl side chain leads the way; and the fact that the carbohydrate glycocalyx that lines the interior of the lysosomal membrane creates a diffusion barrier that would prevent NPC2 from interacting directly with the membrane.[4,10,14] When the L175A/L176A mutation was introduced into full-length NPC1, the protein could not restore egress of cholesterol from lysosomes to a normal degree. These data provide strong support for the notion that cholesterol must be transferred between NPC2 and NPC1(NTD) in order to exit the lysosome. However, the result does not in itself determine whether the transfer goes in the direction of NPC2 to NPC1 or NPC1 to NPC2. In fact, the current *in vitro* data show that the transfer of cholesterol between NPC1 and lipid bilayers facilitated by NPC2 is bidirectional.[12] Regardless of the direction of transfer, what is needed outside of the endosome is a cytosolic sink for cholesterol transferred to NPC1 in the limiting membrane. As for a "tag team effort", loss-of-function mutations in either protein trigger NPC disease. Although the model provides a nice interpretation of the cooperativity between NPC1 and NPC2 in lipid transport, the hypothesis of direct interaction between NPC1 and NPC2 has not been proven, and no physical complex between the two proteins has been yet stabilized.

NPC1 and NPC2 have also found widespread interest due to their involvement in a number of diseases. Most importantly, it is known that 95% of all Niemann−Pick Type C (NPC) patients have one of >200 known mutations in NPC1, while the remainder of the NPC patients have a mutation in NPC2.[17−19] NPC is a recessively inherited neurodegenerative lysosomal storage disease that mostly affects children and is in the vast majority of cases fatal. There is currently no effective treatment approved in the US, even though a number of approaches are currently under investigation.[20−23] In affected individuals, unesterified cholesterol, sphingomyelin, and other lipids accumulate in endosomes and lysosomes of many organs including the brain,[24,25] with most patients developing progressive neurological dysfunction.[26] Recent studies have also found other relevant disease-related roles of NPC1. Cells defective for NPC1 function such as primary fibroblasts derived from human Niemann−Pick type C1 disease patients, are resistant to infection by Ebola virus (EvoV) and Marburg virus (filovirus) but remain fully susceptible to a suite of unrelated viruses.[27,28] The studies demonstrated that NPC1 is essential for EvoV infection. It binds to the virus glycoprotein (GP), opening the possibility of developing new antiviral compounds that interfere with this binding. Resistance of NPC1-deficient cells to EboV is not caused by defects in cholesterol transport in itself, and the precise role of NPC1 in the infection process is not known.

Because of the importance of the correct cholesterol transfer between NPC2 and NPC1 for normal cellular processes as well as for a number of disease states, we decided to investigate the basic biophysical mechanism at the atomistic level. Building on the available crystallographic data and the mutagenesis data, we probed the sliding hypothesis using computational methods. Specifically, we studied here an optimized model of the NPC1(NTD)-NPC2 complex with different positions of cholesterol, as well as its stability and dynamical behavior on the nanosecond time scale that would allow a reorientation of the side chains and loops at the interface of the two proteins. This model can then be used to analyze the binding interface and to understand the structural origin of the effects observed upon mutations at either the binding interface or the cholesterol binding sites. The dynamic behavior of cholesterol in the NPC1(NTD)-NPC2 model was compared with the evolution of the separated moieties (i.e., NPC1(NTD)-cholesterol and NPC2-cholesterol systems). Finally, the pathway of cholesterol transport between the two proteins itself was studied.

MATERIALS AND METHODS

Model Building. The initial models for the NPC1(NTD)-NPC2, NPC1(NTD)/cholesterol-NPC2, and NPC1(NTD)-NPC2/cholesterol complexes have been built from the superposition of the coordinates of the individual X-ray structures containing cholesterol [pdb codes 3GKI and 2HKA] on the working model developed by the group of Professors Brown and Goldstein at UT Southwest Medical Center, which was kindly provided to us. The relative orientation of the proteins in this rigid body alignment was derived from the point mutation experiments that elucidated the putative binding interface.[10,14] From the superposition of the X-ray structures on this model, the initial coordinates have cholesterol in both the NPC1(NTD) and the NPC2 binding pockets. The cholesterol molecules were deleted as necessary to build the starting structures and to study the effect of the presence or absence of cholesterol shown in Figure 1. Short molecular dynamics (MD) simulations (8 ns) were run for each case until stable structures were attained. These equilibrated structures were used to define the starting points for the computational analysis reported in this article. These structures will be referred to as "initial structures" for the remainder of the article. It should be mentioned that several initial models built as described led to dissociation of the complex in a time frame shorter than 8 ns. In these cases, the process has been repeated starting from initial NPC1/NPC2 complexes built by superposition of the individual moieties after dissociation with the Brown and Goldstein model until stable structures were attained. In the simulations, the ionizable residues were set to their normal ionization states at pH 7. The protein atoms, as well as all the water molecules of the crystal structure, were surrounded by a periodic box of TIP3P[29] water molecules that extended 10 Å from the protein. Na^+ counterions were placed by the LEaP module of AMBER11[30] to neutralize the system.

NPC1(NTD) contains 18 cysteine residues (Cys25-Cys74, Cys31-Cys42, Cys63-Cys109, Cys75-Cys113, Cys97-Cys238, Cys100-Cys160, Cys177-Cys184, Cys227-Cys243, and Cys240-Cys247), all of which are known to form disulfide bonds.[10] NPC2, however, has three disulfide bonds connecting residues Cys-8−Cys-121, Cys-23−Cys-28, and Cys-74−Cys-80.[14] These disulfide bonds were manually created *in silico* for the modeling studies in accordance with the available X-ray data. The L175A/L176A and E191A/Y192A mutations were also generated *in silico* using Pymol.

The NPC1(NTD)-cholesterol and NPC2-cholesterol models were similarly built from the coordinates of the available X-ray structures (pdb codes 3GKI and 2HKA, respectively). For the latter, cholesterol sulfate present in NPC2 was converted to cholesterol.

Molecular Dynamics Simulations. The MD simulations were carried out using PMEMD as implemented in the AMBER11 suite of programs.[30] The ff03.r1 version of the all-

dx.doi.org/10.1021/bi4005478 | *Biochemistry* 2013, 52, 6879−6891

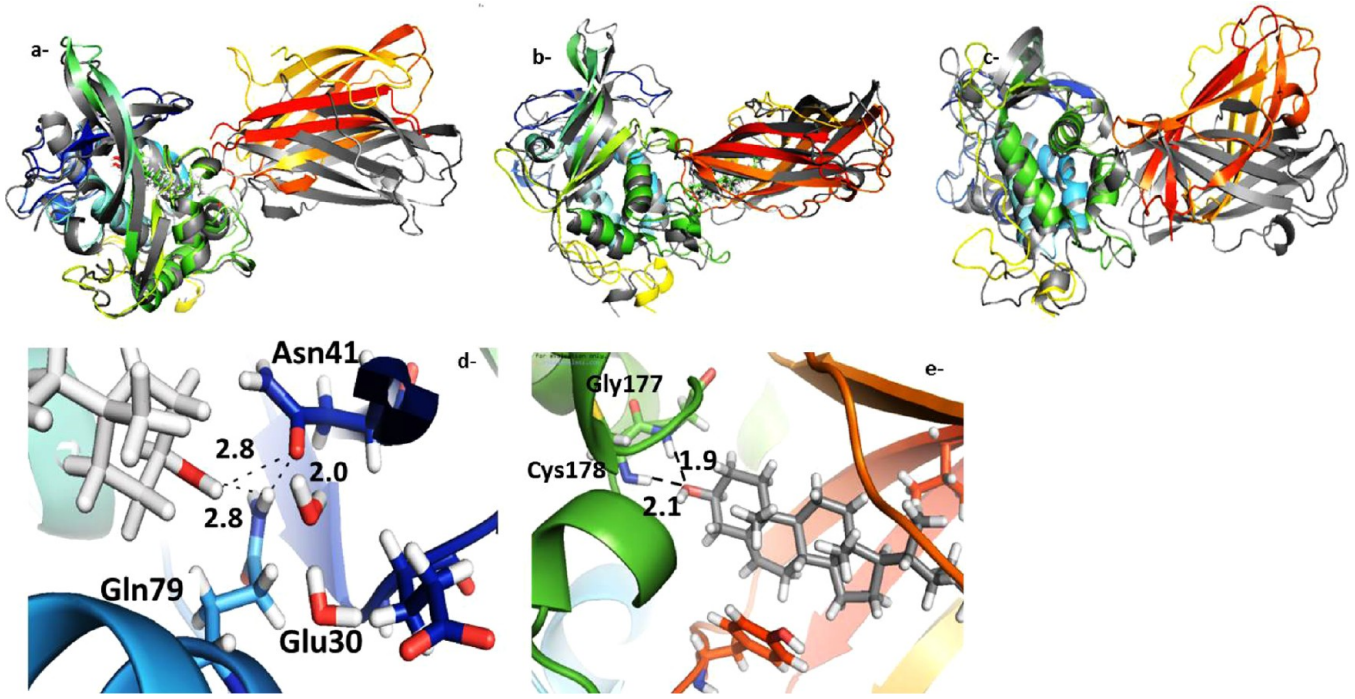

Figure 1. Snapshots at the end of the 86 ns MD simulations showing the evolution of the NP1-NPC2 structures relative to the initial ones (shown in gray) (a): cholesterol in NPC1(NTD) in complete view and (d) close-up of binding site. (b) Cholesterol in NPC2 in complete view and (e) closeup of the binding site. (c) Complex with no cholesterol bound.

atom AMBER force field was used to model the protein and the GAFF force field for the cholesterol ligand.[31,32] Atom-centered partial charges were derived by using the AMBER antechamber program (RESP methodology),[33,34] after geometry optimization at the B3LYP/6-31G* level. In the molecular dynamics simulation protocol, the time step was chosen to be 2 fs, and the SHAKE algorithm[35] was used to constrain all bonds involving hydrogen atoms. A nonbonded cutoff of 10.0 Å was used, and the nonbonded pair list was updated every 25 time steps. Langevin dynamics was used to control the temperature (300 K) using a collision frequency of 1.0 ps^{-1}, with isotropic position scaling to maintain the pressure (1 atm).[36] Periodic boundary conditions were applied to simulate a continuous system. To include the contributions of long-range interactions, the Particle-Mesh-Ewald (PME)[37,38] method was used with a grid spacing of ~1 Å combined with a fourth-order B-spline interpolation to compute the potential and forces in between grid points. The trajectories were analyzed using the PTRAJ module of AMBER.

MM/GBSA, Computational Alanine Scanning, and Per-Residue Decomposition. The MM/GBSA (molecular mechanics-generalized Born surface area) method has been used extensively to investigate protein−protein and protein−ligand interactions.[39−41] It combines the speed of a continuum approach to model solvent interactions with the theoretical accuracy of an MM-based approach to atomistically model protein−ligand interactions. In order to predict the location of hot-spots at interfaces, MM/GBSA has also been used in various alanine-scanning mutagenesis protocols, calculating the relative free energy change ($\Delta\Delta G$) between the wild-type and mutant complex on mutation of an individual residue to alanine[42−44] or calculating the free Gibbs energy of binding on a per-residue basis.[45]

To calculate the Gibbs free energy of binding $\Delta\Delta G_{Bind}$, the Gibbs free energies for the complex, the receptor, and the ligand (ΔG_{Comp}, ΔG_{Rec}, and ΔG_{Lig}, respectively) are calculated individually across a configurational ensemble generated from a molecular dynamics (MD) trajectory and the difference between the complex and the receptor/ligand free energies taken: [46]

$$\langle \Delta\Delta G_{Bind} \rangle = \langle \Delta G_{Comp} \rangle - (\langle \Delta G_{Rec} \rangle + \langle \Delta G_{Lip} \rangle)$$

The configurational ensembles for the complex, receptor, and ligand structures were generated from a single simulation of the complex, from which the unbound receptor and ligand structures were extracted. Following the absolute ΔG calculation, the relative free energy of binding between an alanine scanning mutant and the wildtype complex, $\Delta\Delta G_{Ala}$, is the difference between the ΔG of the mutant and the wild type.

$$\langle \Delta\Delta G_{Ala} \rangle = \langle \Delta G_{Mut} \rangle - \langle \Delta G_{Wild} \rangle$$

For the different systems studied here, the MM/GBSA calculations used 500 frames saved over 76 ns, extracted between 10 and 86 ns of the NPC1(NTD)-NPC2, NPC1-(NTD)-cholesterol/NPC2, and NPC1(NTD)/NPC2/cholesterol MD runs. MM contributions were calculated with a dielectric constant of 1.0 and an interaction cutoff of 999 Å. GB solvation energies were calculated with an internal dielectric constant of 1.0 and an external constant of 80.0. The nonpolar contribution to solvation energy was calculated as $G_{NONPOL} = \gamma SASA$, with γ set to 0.0072 kcal mol^{-1} $Å^{-2}$ and SASA as the Connolly surface calculated with the Molsurf program with a solvent probe radius of 1.4 Å and Bondi atomic radii. For the calculation of relative free energies between a set of closely related complexes, it is often assumed that the entropic contributions to the absolute free energies cancel each other out. Since this approximation does not strictly yield the free energy, the calculated values are referred to as binding energies. We therefore used the methods to help understand the

dx.doi.org/10.1021/bi4005478 | *Biochemistry* 2013, 52, 6879−6891

experimental predictions derived from the alanine scanning of the NPC1(NTD)-NPC2 interface.

Nudged Elastic Band Calculations. The nudged elastic band (NEB)[47] method, as implemented in AMBER11, was employed to investigate the pathway for cholesterol transfer between the NPC1(NTD)-NPC2/cholesterol and NPC2-NPC1(NTD)/cholesterol structures. The structures stabilized after MD simulations as described above were used as end points in NEB calculations. Thirty replicas were generated where the first 15 images were started as the initial conformation (cholesterol in NPC1(NTD)), and the last 15 images were started as the final conformation (cholesterol in NPC2). The simulated annealing protocol involved heating the system to 500 K over 5 ns, followed by slow cooling over additional 5 ns, followed by quenched dynamics to remove excess kinetic energy from the system. A generalized Born (GB)[48,49] implicit solvation model was used in the NEB calculations with a nonbonded and GB radii cutoff of 15 Å and without Debye−Hückel screening. Langevin temperature scaling with a collision frequency of 1000 ps and SHAKE was used.

RESULTS AND DISCUSSION

Structure of the NPC1(NTD)-NPC2 Complex. The initial working models built are based on a rigid body docking of two independently obtained X-ray structures with cholesterol in both binding sites. However, in the real system, only one of the two domains of the NPC1(NTD)-NPC2 complex contains a cholesterol molecule. This will lead to changes in the protein complex, especially at the binding interface and the cholesterol binding site, as is indicated by the fact that most trajectories started from the initial working model lead to dissociation of the complex. To provide a more refined model of the complexes that allows a better analysis of the interactions than what can be provided by the rigid model, we studied three NPC1(NTD)-NPC2 complexes: (i) cholesterol in the NPC1-(NTD) pocket, (ii) cholesterol in the NPC2 pocket, and (iii) no cholesterol. The structures, dynamics, and stability of the three complexes were studied by following their evolution over ~86 ns using MD simulations in both explicit and implicit solvents to refine the models. In order to analyze the effect of the NPC1(NTD)−NPC2 interface on cholesterol binding, we also analyzed the separated NPC1(NTD)-cholesterol and NPC2-cholesterol systems. The corresponding apo structures of NPC1(NTD) and NPC2 were studied using 40 ns MD simulations, which is considered sufficient for a system where no dissociation event can occur.

Shown in Figure 1a−c are the structures at the end of the 86 ns explicit solvent MD simulations of the NPC1(NTD)-NPC2 complex with the cholesterol in the NPC1(NTD) binding site and the NPC2 binding site, and no cholesterol, respectively. Close-ups of the cholesterol binding in NPC1(NTD) and NPC2 are shown in Figure 1d and e, respectively. For comparison, the changes occurring in the cholesterol binding site of NPC1(NTD) and NPC2 individual structures can be seen in Figure S1 and S2 in the Supporting Information. Figure S4 (Supporting Information) shows the distances in the three complexes studied as a function of simulation time. It can be seen that the major changes over the course of the simulation occur in the NPC1(NTD)-NPC2 complexes when no cholesterol is present and when the cholesterol molecule is located in the NPC1(NTD) part (left in Figure 1a and Figure 2).

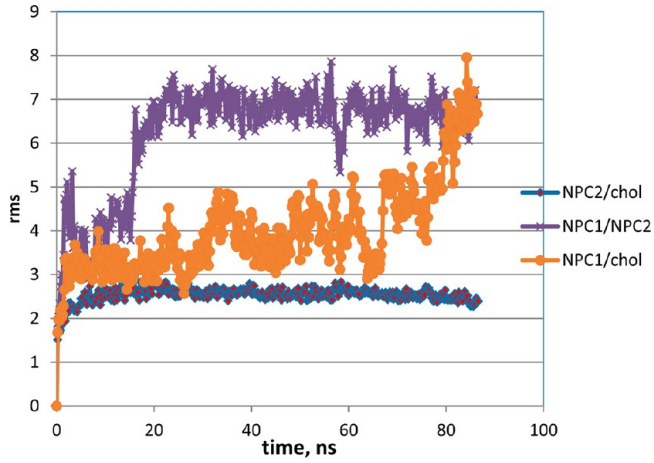

Figure 2. rmsd for NPC1(NTD)-NPC2 (purple), NPC1(NTD)/cholesterol-NPC2 (orange), and NPC1(NTD)-NPC2/cholesterol (blue) complexes over time.

As described for the X-ray structure[10] and seen in the MD simulations of NPC1(NTD)-cholesterol, the buried OH group is stabilized in the NPC1(NTD)-cholesterol/NPC2 complex by H-bond interactions with Asn41, Gln79, and Glu30, which also impose stereospecificity. The interactions alternate between direct and through-water hydrogen bonding of Asn41-cholesterol and Gln79-cholesterol over the MD run, with average distances of 2.5 and 2.6 from Asn41 and Gln79, respectively, to the hydroxyl oxygen atom of cholesterol. The interactions are always through-water for the case of Glu30. The hydrogen bonding network is reinforced by Asn41-Gln79 H-bond interactions (average distance 2.7 Å). These interactions are in agreement with the findings of the alanine scan mutagenesis, which showed 90% and 40% reduction in cholesterol binding when Asn41 and Gln79 were mutated, respectively.[10,14] However, the lipophilic end of the cholesterol molecule interacts with Pro101 (NPC2), which is also establishing lipophilic contacts with Leu153 (NPC1). Other stable interactions involve Ser146(NPC1) and Glu99(NPC2), whereas the Tyr192(NPC1)−Met60(NPC2) interaction, which is stable in the absence of cholesterol, is disrupted in the NPC1(chol)/NPC2 system as a consequence of the shift of the β-strands of NPC2 that changes the interactions at the interface. A narrowing of the NPC2 opening in the absence of cholesterol is observed when comparing the NPC2-cholesterol structure with the apo NPC2, which occurs as a consequence of the repositioning of Leu94, Phe-66, Tyr-100, and Pro-101 (Figure S1, Supporting Information). In the NPC1(NTD)-cholesterol/NPC2 complex, this narrowing occurs in the early stage of the equilibration process and cannot be monitored during the 86 ns production MD. A narrowing of the pocket can be observed, however, indicated by the comparison of the structures of the NPC1(NTD)-cholesterol/NPC2 and NPC1-(NTD)-/NPC2 complexes at the end of the MD simulations with the available NPC2 crystal structures 1NEP (no ligand) and 2HKA (Figure 3a). The strands in the first β-sheet (βA, βB, and βE) are closer in our model to 1NEP (purple) than to 2HKA (gray), from which the initial model was built showing the evolution of the NPC2 moiety to a structure where no ligand is present.

When cholesterol fills the NPC2 pocket, it also interacts with residues of NPC1(NTD). It moves toward the interface, gaining stability from hydrogen bond interactions of the

dx.doi.org/10.1021/bi4005478 | Biochemistry 2013, 52, 6879−6891

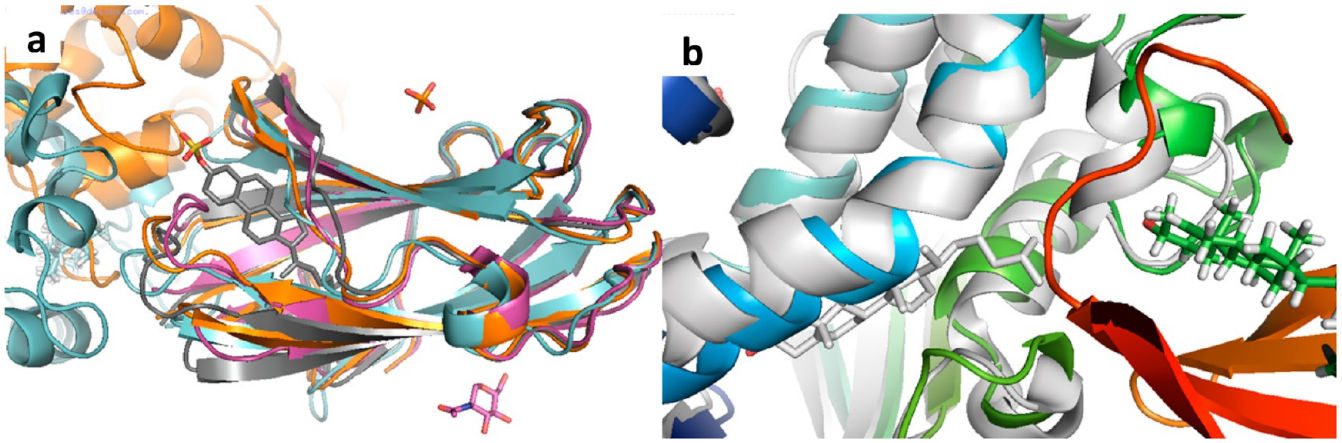

Figure 3. (a) Superposition of the NPC1(NTD)-NPC2 (orange) and NPC1(NTD)-cholesterol/NPC2 (light blue) complexes at the end of the simulation with the NPC2 available X-ray structures 1NEP (purple) and 2KHA (gray). Only the NPC2 moiety is shown. (b) Superposition of the 86 ns snapshot of the NPC1(NTD/NPC2)-cholesterol complex with the NPC1(NTD)-cholesterol Xray structure (3GKI) (white) showing the opening of helixes 7 and 8 (green) in the complex.

cholesterol hydroxyl group with the backbone NH of residues Cys177(NPC1) and Gly178(NPC1) (Figure 1d). This interaction may also influence the movement of the loop between helices 7 and 8, triggering the opening of the NPC1(NTD) pocket (Figure 3b). The helices and the loop between them (shown in green in Figure 1b) are responsible for expanding the opening and allowing cholesterol to enter or exit the binding pocket of NPC1(NTD). Helix 3 (light blue in Figure 1b) also contributes to the expansion, with the largest shift close to the rim of the opening (Figure S2 in Supporting Information). The movement of the helices mainly occurs in the equilibration stage but can still be noticed in the production phase of the MD, as shown by monitoring the Cys78-Pro68 and Leu83-Leu65 distances over time (see Figure S3, Supporting Information). A significant shift in the position of the α-helices, mainly helix 7, helix 3, and helix8, has been also noticed from the comparison of the NPC1(NTD)-cholesterol complex and the apo structure, both experimentally and from the analysis of the MD runs. In both cases, the largest shift was found at Leu87 due to the interaction of the methyl group in the isooctyl side chain of cholesterol with Leu87 (Figures S2 and S3, Supporting Information). However, the interaction of cholesterol with residues of NPC1 keeps the interface stable, as can be deduced from the distance between residues in the two moieties (Figure S4, Supporting Information). When no cholesterol is present in either protein (Figure 1c), the interface changes to increase the Ser146(NPC1)/Glu99(NPC2) distance. The RMS increases during the MD in a similar way as the one observed for the NPC1(cholesterol)/NPC2 complex (Figure 2).

The large changes observed in the simulations of the NPC1(chol)-NPC2 and the cholesterol-free complex suggest a role of cholesterol for the stability of the NPC1(NTD)-NPC2 complex. The evolution of those systems may be indicative of an onset of dissociation, which may occur over longer periods of time than those that can be modeled in MD simulations. In order to work as a "tag team duo," the two proteins can just associate as a transient with a half-life just enough to allow the transfer of cholesterol between them.

As mentioned before, binding of cholesterol to the NPC2 pocket adds additional stability to the system through the interaction of the cholesterol isooctyl chain with lipophilic residues of the cavity and simultaneous hydrogen bonding of the cholesterol hydroxyl group with the backbone NH of residues Cys177 and Gly178 of NPC1(NTD). As a result, the NPC1(NTD)-NPC2/cholesterol system remains stable during 86 ns of MD simulation (Figure 2).

The comparison of the apo NPC1(NTD) X-ray structure (pdb code 3GKH) with the NPC1(NTD) moiety of the NPC1(NTD)-NPC2 and the NPC1(NTD)-NPC2/cholesterol complexes shows a perfect overlap, with backbone rmsd of 1.4 Å and 1.6 Å, respectively (Figure S5, Supporting Information). A minor change in helix 7 to accommodate to the interface can be noticed, together with fluctuations in mobile loops. However, when cholesterol binds to the NPC1 pocket in the reverse orientation, lipophilic interactions of the isopropyl end with residues of the NPC1 surface compete with the interactions between the NPC units.

Stability of the NPC1(NTD)-NPC2 Complex. The NPC1(NTD)-NPC2 complex modeled above has never been observed directly, indicating that the binding energy for the protein−protein interaction is low. This is in agreement with the results of the MD simulations, which clearly show the dissociation of the two components of the complex before ~80 ns (orange in Figure 2). The 86 ns simulation allows the analysis of the residues that stabilize the transient NPC1-(NTD)-NPC2 complex, which has never been observed directly. To estimate the stability of the NPC1(NTD)-NPC2 complex, we performed MM/GBSA calculations on snapshots derived from the MD simulations using the MM/GBSA postprocessing module of AMBER11.[30] Before discussing these results in detail, it should be pointed out that the precise calculation of the NPC1(NTD)-NPC2 interaction energy is complicated by several factors. The main concern is that the evaluation of the interactions between residues has been done over bonded conformations. As was observed in several other cases,[50] this leads to an overestimation of the absolute value of the binding energy. Keeping this in mind, the analysis of the relative rather than absolute binding energies provides valuable information to rationalize the influence of cholesterol and/or mutations in the binding and to identify the residues that have large contributions to it. Therefore, the MM/GBSA contribution per residue to the binding energy has been calculated for

dx.doi.org/10.1021/bi4005478 | *Biochemistry* 2013, 52, 6879−6891

the different models. The results of these studies are shown in Table 1.

Table 1. Contribution of the Most Relevant Residues to the Binding Energy As Derived from the MM/GBSA per Residue Decomposition in kcal/mol[a]

Residue number	NPC1(NTD) -NPC2	NPC1(NTD)- NPC2/cholesterol	NPC1(NTD)/ cholesterol-NPC2
Val59 (NPC2)	-1.07	-2.91	-0.9
Met60 (NPC2)	-4.3	-6.43	-3.5
Ile62 (NPC2)	-177	-1.96	-1.6
Val64 (NPC2)	-1.11	-2.07	-1.3
Tyr100 (NPC2)	-1.04	-2.7	-0.69
Pro101(NPC2)*	**-3.1**	**-3.4**	**-2.09**
Ser102 (NPC2)	-0.8	-0.8	-0.24
Ile103 (NPC2)	-3.1	-3.66	-1.20
Leu175 (NPC1)	-1.92	-3.01	-1.15
Leu176 (NPC1)	-0.01	-2.39	-0.13
Cys177 (NPC1)	-0.11	-1.18	0.32
Gly178 (NPC1)	-0.08	-1.32	-0.12
Lys179(NPC1	-1.0	-0.3	-0.1
Tyr192 (NPC1)	-2.45	-2.68	-1.83
Cholesterol	-------	-8.75	-0.4
Total	-20.5	-33.0	-7.4

[a]Red letters denote residues that when mutated to alanine decrease the amount of [3H]cholesterol transferred by >60% relative to the average of the WT values obtained in 3 experiments. Blue letters denote residues that when mutated to alanine decrease binding by >85%.[9,13]*, residue Pro101 was identified as essential for both binding and transfer.[11] No experimental data were available for Ser102 and Cys177.

In the absence of cholesterol, the total MM/GBSA calculated NPC1(NTD)-NPC2 binding energy is −22.5 kcal/mol, which greatly overestimates the absolute value of the binding energy for the reasons discussed above but is useful as a baseline. In the per-residue decomposition, large contributions are associated with Tyr192(NPC1(NTD)), Met60 (NPC2), Leu175(NPC1-(NTD)), Pro101(NPC2), and Ile103(NPC2), followed by Val59(NPC2), Ile62(NPC2), and Val64(NPC2) residues (Table 1). Several of these interactions are of interest because they are observed in the MD-refined model but not in the initial rigid body model, emphasizing the importance of the reorganization of the interface upon binding. In turn, the contributions from residues not in the interfacial region are predicted to be negligible, in line with the experimental observations from the mutagenesis studies.[14] The structure stabilized after MD simulations shows a nonbonded interaction between the Met60 sulfur atom and the aromatic ring of Tyr192, reinforced by lipophilic interactions of Leu175 with Pro101. Ile103, Val59, Ile62, and Val64 also contribute to the lipophilic stabilization (Figure 4a). A lipophilic interaction between Tyr100 (NPC2) and Lys179(NPC1) is also observed. These results are in good agreement with the available experimental data with respect to correctly identifying residues that do and do not contribute to binding,[10,14] increasing the confidence in the refined model and in turn providing insights into the structural origin of the observations which cannot be derived from the mutagenesis results alone.

Mutagenesis experiments have shown that Tyr192Ala and Leu176Ala mutations significantly decrease the NPC1(NTD)-NPC2 cholesterol transfer to less than 25% of bound cholesterol transferred to liposomes, which has been interpreted as a failure to form the protein−protein complex as a result of the mutation.[10] The Tyr100Ala, however, gave binding values of 8% of the wild type.[10] The Val59Ala mutant was also found partially defective in the transfer of cholesterol, whereas the Val64Asp mutant was found severely defective.[14] This Asp mutation significantly changes the lipophilicity of the NPC2 pocket, making the interaction with cholesterol less favorable. The Tyr100, Val59, and Val64 have been found relevant for cholesterol binding.[13]

As a further test for the "sliding model,"[10] which postulates a transfer from NPC2 to NPC1(NTD), and the hypothesis that cholesterol binding increases the formation of the NPC2-NPC1(NTD) complex, the binding energy of the NPC2/cholesterol complex to NPC1(NTD) was evaluated using the same methodology. The same residues calculated to have a large contribution in the MM/GBSA stabilization for the NPC2-NPC1(NTD) system were found, with additional residues contributing through interactions with cholesterol itself, either lipophilic or hydrogen bonding interactions with the cholesterol hydroxyl end (Figure 4). This additional stabilization increases the MM/GBSA calculated binding of NPC2-cholesterol to NPC1(NTD) by 13.5 kcal/mol relative to the NPC1(NTD)-NPC2 binding when no cholesterol is present. This increase can be rationalized by the two additional hydrogen bonds formed between the hydroxyl end of the cholesterol molecule in the NPC2 pocket, and the residues in NPC1(NTD) (see Figures 1e and 4b).

According to the MM/GBSA per-residue decomposition energy, the contribution of Leu176 (NPC1(NTD)) to the binding increases to 2.39 kcal/mol when cholesterol fills the NPC2 pocket, as it interacts more strongly with Pro101 (NPC2). The interaction of Tyr100 with Lys157 is disrupted by the presence of the cholesterol molecule, with Tyr100 reoriented to line the cholesterol pocket. Gly178 participates now in the binding, with a contribution of 1.32 kcal/mol, which was negligible in the absence of cholesterol. The contribution of Tyr192(NPC1(NTD)) does not change markedly, whereas the one from Met60(NPC2) increases slightly to 6.5 kcal/mol. Cholesterol itself has a large contribution (8.75 kcal/mol), associated with its interaction with residues of NPC1(NTD).

Cholesterol binds efficiently to the NPC1(NTD) active site pocket of the cholesterol-NPC1(NTD)/NPC2 complex

dx.doi.org/10.1021/bi4005478 | Biochemistry 2013, 52, 6879−6891

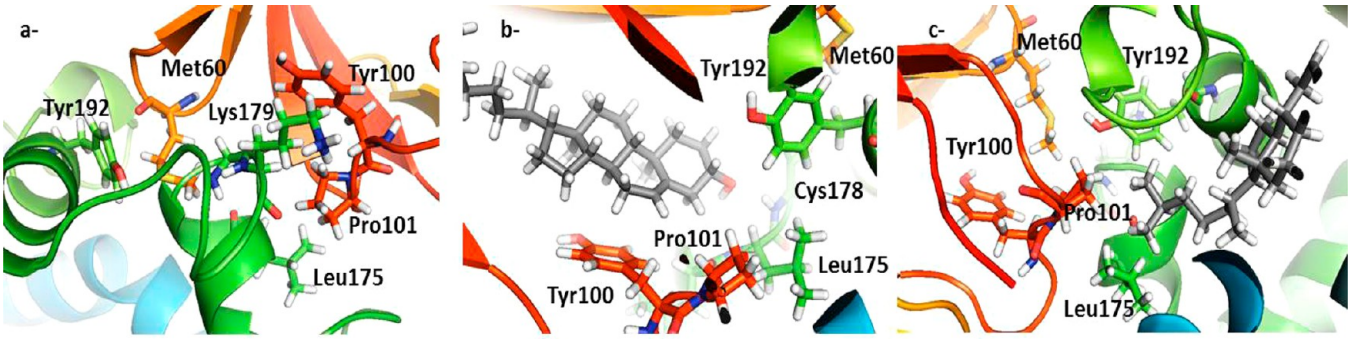

Figure 4. Residues involved in stabilizing interactions in the interface of the (a) NPC1(NTD)-NPC2 complex; (b) NPC1(NTD)-NPC2/cholesterol complex; and (c) NPC1(NTD)/cholesterol-NPC2 complex.

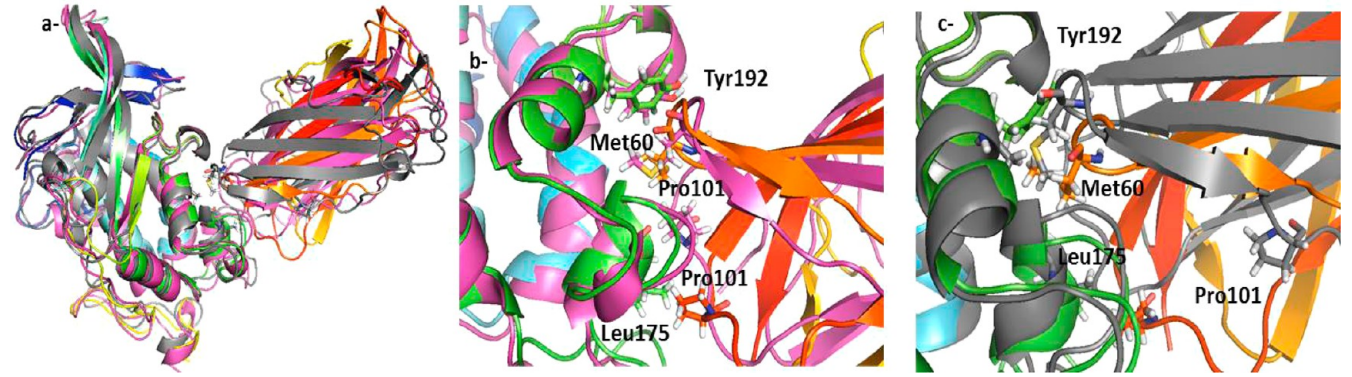

Figure 5. Influence of mutations on the evolution of the NPC1(NTD)-NPC2 systems. The nonmutated complex is overlaid with the L175A/L176A (purple) and E191A/Y192A (gray) mutated ones in the figure on the left (a). Residues at the interface are highlighted as sticks in the zoomed in view of the L175A/L176A mutated complex (b) and of the E191A/Y192A mutated one (c).

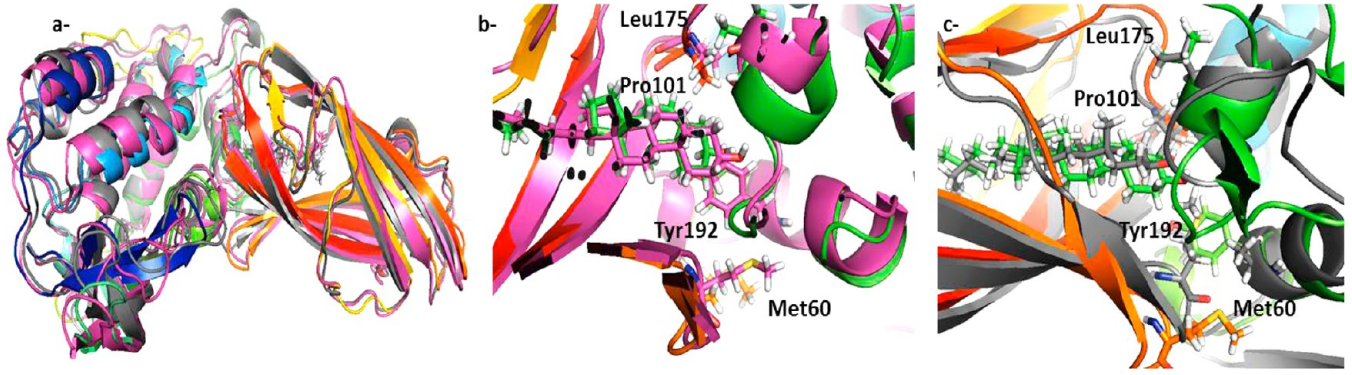

Figure 6. Influence of mutations on the evolution of the NPC1(NTD)-NPC2/cholesterol complex. (a) Nonmutated complex overlaid with the L175A/L176A (purple) and E191A/Y192A (gray) mutants. Residues at the interface for the (b) L175A/L176A mutant complex and (c) E191A/Y192A mutated complex.

through interactions with Asn41, Gln79, and Glu30 (Figure 1d). Nevertheless, the binding does not reinforce but rather weakens the NPC1(NTD)-NPC2 interaction. The lipophilic end of the cholesterol molecule is positioned in a lipophilic pocket defined by Tyr192 (NPC1(NTD)), Leu176 (NPC1-(NTD)), and Leu175 (NPC1(NTD)). The interaction of cholesterol with Tyr192 and Leu176 decreases the stability of the NPC1(NTD)-NPC2 system, as it disrupts the lipophilic interactions (Tyr192-Met60 and Leu176-Pro101) in the interface of both moieties (Figure 4c). The contributions of these residues to the binding decrease markedly, as shown in Table 1. In agreement with these observations, the cholesterol-NPC1(NTD)/NPC2 complex shows a large distortion of the interface and a rms value close to 8A at the end of the simulation (Figure 2). This provides a rationalization of the previously unexplained directionality of the cholesterol transport as discussed below.

Effect of the L175A/L176A and E191A/Y192A Mutations. Recent alanine scanning mutagenesis studies have identified L175A/L176A and E191A/Y192A as the two mutants most deficient in NPC2-mediated cholesterol transfer from NPC1(NTD) to liposomes.[10] The transfer defect was associated with a defective interaction of NPC1(NTD) with NPC2 and not with liposomes. In order to provide a structural basis for this observation, we modeled the two mutations *in silico* and analyzed the influence of the mutations on both the

dx.doi.org/10.1021/bi4005478 | *Biochemistry* 2013, 52, 6879−6891

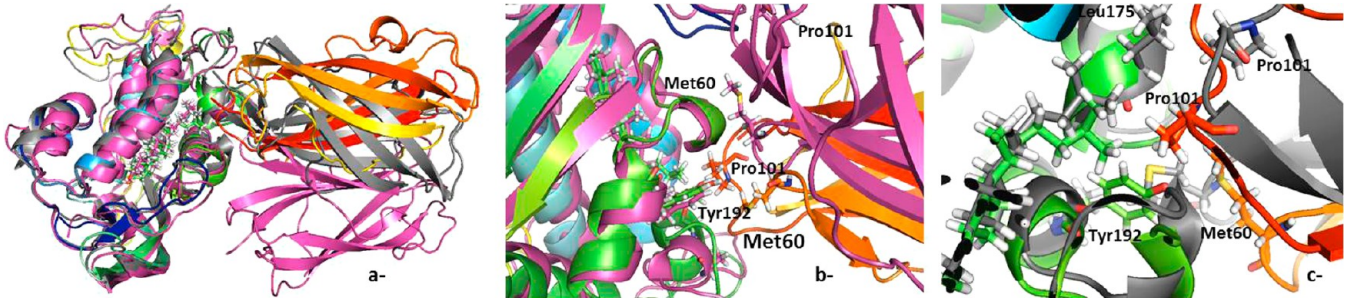

Figure 7. Influence of mutations on the evolution of the NPC1(NTD/cholesterol)-NPC2 complex. (a) Nonmutated complex overlaid with the L175A/L176A (purple) and E191A/Y192A (gray) mutants. Residues at the interface for the (b) L175A/L176A mutant complex and (c) E191A/Y192A mutated complex.

stability of the NPC1(NTD)-NPC2 associated structures and on cholesterol transport. Starting from the refined model discussed above (structures shown in white in Figure 1), the L175A/L176A and E191A/Y192A mutants were generated *in silico* and studied analogously using 86 ns MD simulations for the cases when no cholesterol was present and when it was bound to either the NPC1(NTD) or the NPC2 pockets.

The MD simulations clearly show that the NPC1(NTD)−NPC2 interface distorts after the introduction of the L175A/L176A and E191A/Y192A mutations (see Figure 5). The L175A/L176A mutation (Figure 5b) disrupts the interaction of Leu175 with Pro101. According to the MM/GBSA per-residue decomposition energy, these residues contribute 1.98 and 3.9 kcal/mol to NPC1(NTD)-NPC2 binding, respectively. The E191A/Y192A mutation (Figure 5c) disrupts the Tyr192−Met60 interaction previously discussed, leading to a distortion of the interface as the Met residue tends to occupy the space previously filled by Tyr192. These residues were found to contribute 4.3 and 2.45 kcal/mol, respectively, to the MM/GBSA calculated NPC1(NTD)-NPC2 binding. Their interaction is reinforced by the adjacent Ile103, Val59, Ile62, and Val64 residues, which also show significant per-residue contributions in the MM/GBSA energy decomposition. In comparison, the contribution of other residues is negligible. This description of the interactions is also supported by the results of the *in silico* alanine scanning, which show a decrease of 26% in the binding energy when Tyr192 is mutated to Ala and 6.5% when Leu175 is mutated to Ala. These mutations were experimentally found to decrease cholesterol transfer by more than 25%.[10]

The L175A/L176A and E191A/Y192A mutations have a minor effect on the NPC1(NTD)-NPC2 complex with cholesterol bound to NPC2 (Figure 6), as the stabilizing interactions of the cholesterol OH with the backbone NH of residues Cys177 and Gly178 shown in Figure 1e are conserved. Although these residues are not mutated, they are in close proximity to the L175A/L176A and E191A/Y192A ones, slightly increasing the rms values (Figure S6, Supporting Information) relative to those in the nonmutated complex (Figure 2). The reduction in binding energy calculated by the MM/GBSA alanine scanning is similar to the one previously reported for the NPC1(NTD)-NPC2 system: 20% for the Tyr192Ala mutation and 10% for the Leu175Ala mutation.

The nonmutated NPC1(NTD)-NPC2 complex with cholesterol bound to NPC1(NTD) showed an important reorganization in the interface (Figure 1a), in agreement with the lower binding energy between both moieties derived from the MM/GBSA calculations (Table 1). Accordingly, this complex is the most strongly affected by the L175A/L176A and E191A/Y192A mutations among the models studied here. As was described previously, the lipophilic moiety of cholesterol is surrounded by Leu175, Leu176 (NPC1(NTD)), and Tyr192-(NPC1(NTD)) (Figure 4c), decreasing the availability of the residues to interact with NPC2. In the time scale studied here, the effect is more important for the L175A/L176A mutation, leading to a faster destabilization of the interface (Figure S6, Supporting Information). As a result of this destabilization, we do not expect either mutant to form a stable complex.

Similarly, the results of the simulations of the mutant NPC1(NTD/cholesterol)-NPC2 complex (Figure 7) are in agreement with the results of the MMGBSA calculations, which show a decrease in the NPC1(NTD)-NPC2 binding energy when cholesterol binds to the NPC1 pocket, in line with a smaller per residue contribution to the total binding energy (Table 1).

Model for the Mechanisms of Cholesterol Transfer between NPC1(NTD) and NPC2. MD simulations provide important insights into conformational flexibility but are often limited to time scales of the order of tens of nanoseconds. Many biochemically interesting processes, including the cholesterol transport discussed here, occur at much slower time scales and can therefore not be simulated directly. Several methods have been developed to examine such processes. Among them, the NEB method allows the localization of complex transition paths (and the corresponding energy barriers) given only initial and final states of a reaction, conformational change, or any nontrivial path for macromolecules.[47] In NEB calculations, the path for a conformational change is quantified with a series of images of the molecule spaced along the path. In short, the images of the starting and end points of the process, in our case the structures with cholesterol in either the NPC1(NTD) or the NPC2 binding pocket, are fixed in space. Each image in-between is connected to the previous and next image by virtual "springs" along the path that keep each image from sliding down the energy landscape onto adjacent images. The path represents the trajectory that a molecule follows through the particular change, and this path can be derived independently of the time scale for the conformational change. The advantage of this method is that in principle, it only depends on the structures of the starting and end points, and unlike the use of biasing potentials, it does not assume a specific minimum energy pathway along a simple coordinate. This method has been successfully applied to a number of biological processes of similar complexity.[51,52]

We have used the NEB approach to model the pathway for cholesterol transfer between the NPC1(NTD) and NPC2

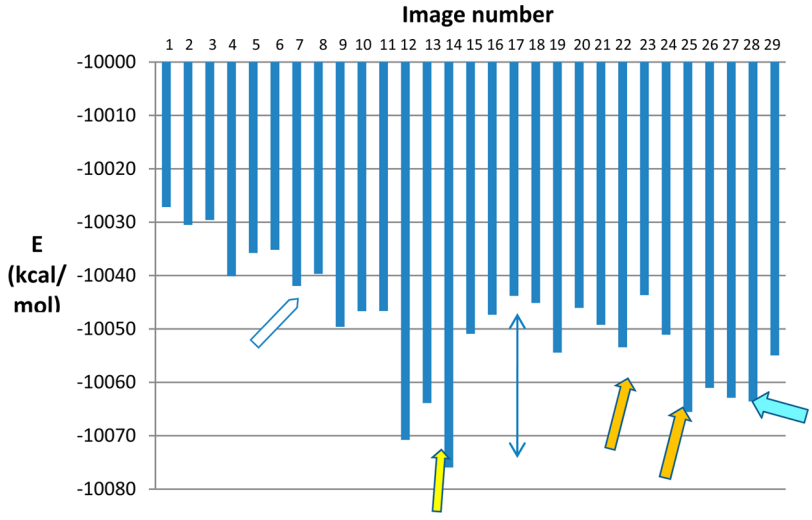

Figure 8. Variation of the potential energy (kcal/mol) along the NEB-proposed pathway. Arrows indicate the images shown in Figure 9, discussed in more detail in the text. The colors of the arrows match the colors of the cholesterol molecule in the images shown in Figure 9 for different steps of the transfer.

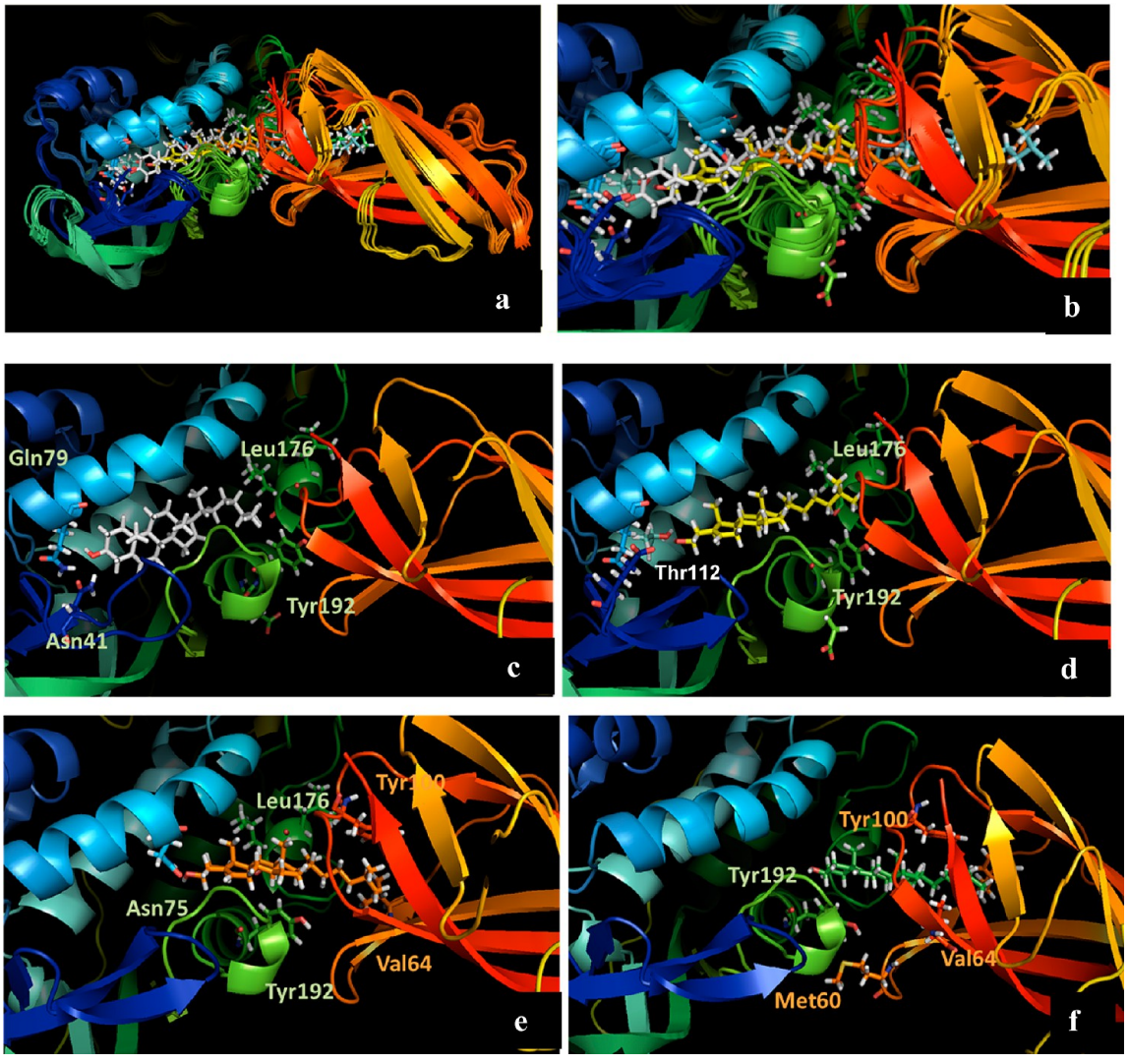

Figure 9. (a) Superposition of snapshots associated with energy minima (arrows in Figure 8) in the transfer of cholesterol between NPC1(NTD) and NPC2. (a) Entire view of the NPC1-NPC2 system. (b) Closeup of the cholesterol molecule during the transfer. (c–f) Snapshots of relevant steps of cholesterol transfer.

dx.doi.org/10.1021/bi4005478 | *Biochemistry* 2013, 52, 6879–6891

active site pockets, using AMBER11. The converged NPC1-(NTD)-NPC2 structures from the MD simulations (after 30 ns MD simulation runs), having a cholesterol molecule in either the NPC1(NTD) (Figure 1a) or the NPC2 (Figure 1b) pocket, were used to define the initial and final states for the simulation of its transfer, respectively. A total of 30 replicas were generated where the first 15 images were started as the initial conformation (cholesterol in NPC1(NTD)) and the last 15 images were started as the final conformation (cholesterol in NPC2). The convergence of several simulated annealing/quenching dynamics protocols were compared, using both 30 and 12 replicas. The results shown here were derived from a protocol using simulated annealing to 500 K over 10 ns, followed by 2 ns quenching dynamics.

For the NEB calculations, the images along the pathways showed different steps for the transfer of cholesterol between NPC1(NTD) and NPC2. This NEB pathway thus provides a model for the minimum energy pathway for the cholesterol transfer mechanism (Figure 8). Representative minima in the pathway are shown in Figure 9, with the cholesterol molecule colored in the sequence of the reaction pathway from NPC1(NTD) to NPC2 as white, yellow, orange, and cyan. It can be seen in Figure 8 that five clear defined structures (marked by arrows in Figure 8) can be identified. These structures can be thought of as stepping stones along the cholesterol transfer pathway as identified by the NEB calculations.

The analysis of the structural snapshots shows that the first 8 replicas correspond to the closely related coordination modes of cholesterol in the NPC1(NTD) pocket. For this conformation (Figure 9c), the coordination of the OH terminus of cholesterol remains essentially the same as shown in Figure 1d, with the lipophilic end positioned between Tyr192 and Leu176. The difference between the replicas lies in the conformation of the protein, adopting a conformation suitable for cholesterol transfer. The conformational changes necessary include the movement of helix 3 (shown in light blue in Figure 1) discussed previously by Brown and Goldstein[10,11] but also a significant change in the loop and short helix region of NPC1(NTD) containing residues 162−186 (shown in green in Figure 1), which have been described as responsible for opening the NPC1 pocket to allow the transfer.

A second distinguishable coordination along the NEB pathway (shown in yellow, image #14, Figure 8), is stabilized by a hydrogen bond of the cholesterol hydroxyl group with Thr112, triggering a small displacement of helix 3 at the bottom of the NPC1 channel. Interaction with this Thr112 residue has been mentioned before as an alternative and favorable interaction.[10] The lipophilic end has moved ∼4 Å into NPC2, reinforcing lipophilic interactions with Tyr192, Leu175, and Leu176 and pushing away helix 7, helix 8, and the adjacent loop (shown in green in Figure 1), widening the NPC1(NTD) exit (Figure 9d). It is worth noting that this structure is predicted to be more stable than the structure with cholesterol deeply buried in the NPC1(NTD) part, presumably because it engages in interactions with both NPC1(NTD) and NPC2. These interactions can of course not be observed in the crystal structures of the separate units, indicating the limitations of conclusions about the protein−protein complex that can be drawn from the separate structures. It also provides a structural rationale as to why the protein−protein complex could be stabilized by the presence of cholesterol.

In the structure shown in orange (image #22, Figure 8), the cholesterol OH interacts with Asn86, and the lipophilic end lies deep enough in NPC2 to interact with a lipophilic pocket defined by Tyr100, Val59, and Val64 (Figure 9e). Helix 3 is further displaced inward, showing a maximum shift at residue Asn75 (1.5 Å at C_α), which reorients to interact with cholesterol. The entrance of cholesterol in the NPC2 cavity originates a widening of the interface, which becomes visible in the shifting of helix 7, where Leu175 moves 1.3 Å (measured at C_α).

The lipophilic interactions of cholesterol and NPC2 residues are better defined in image #25, which is more stable than image #22. These lipophilic interactions are the only ones holding cholesterol in image #27, where the two moieties are still held together by interactions previously described as Tyr192(NPC1)-Met60(NPC2) (Figure 9f). In the conformation shown in image #28, the interactions mentioned before for the NPC2/cholesterol-NPC1(NTD) system (Figure 1e) are already stabilized. The interactions for the initial and final stages, shown in white for cholesterol in NPC1(NTD) and cyan for cholesterol in NPC2, respectively, are those in Figure 1d and e.

Before discussing the energies calculated along the NEB path shown in Figure 8, it should be pointed out that the energies have to be considered approximate, as they are dependent on the number of replicas and the time each replica is equilibrated at a given temperature. A similar calculation, using 12 replicas, rendered the same pathway, but larger energy differences were calculated. A potential source of error may be also originated in the use of a generalized Born (implicit) solvent model, as the interactions in the different steps might be stabilized by explicit water molecules. The NEB calculations result in a system more stable when cholesterol occupies the NPC2 pocket than when it is deeply buried in the NPC1(NTD) one. This is in agreement with the energy difference of 28 kcal/mol between the minimized structures used as initial and final conformations, which favors the cholesterol/NPC2-NPC1(NTD) structure over the cholesterol/NPC1(NTD)-NPC2 one. As discussed earlier, the calculations indicate that the most stable position of cholesterol in the complex is best represented by image #14, which allows for interactions with both NPC1(NTD) and NPC2. The relative energies of this image indicate that cholesterol will be predominantly located in NPC1(NTD) but allows for the experimentally observed bidirectional transfer cholesterol.[12] The largest increase in energy that has to be overcome in the transfer is associated with the jump from image #14 to image #17 and may be associated with the opening of the pocket to allow cholesterol transfer (Figure 10).

In considering the overall directionality of the cholesterol transfer, it is worth noting that based on the MM/GBSA calculations, cholesterol binding to NPC2 stabilizes the NPC1(NTD)-NPC2 system, whereas its binding to NPC1 has the reverse effect. This may be indicative of the formation of a cholesterol/NPC2-NPC1(NTD) complex that releases cholesterol to the membrane after its transfer to NPC1(NTD), as the NPC1(NTD)-NPC2 system is more stable than the cholesterol/NPC1(NTD)-NPC2 one (Table 1). Finally, any model based on NPC1(NTD) does not consider the transfer of cholesterol through the membrane, which acts as an effective thermodynamic sink shifting the equilibrium toward the transport of cholesterol from NPC2 and NPC1 as observed in the biological system.

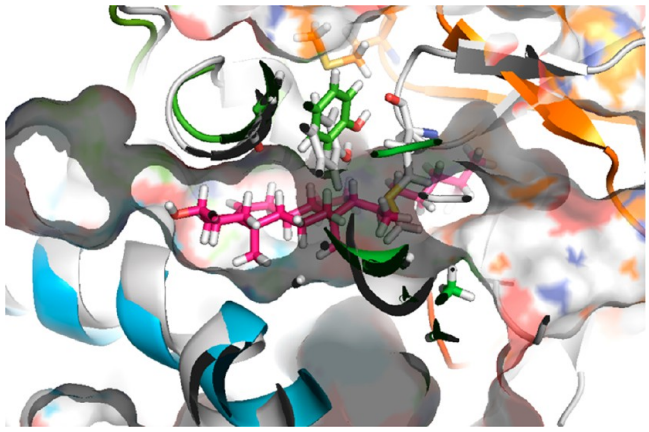

Figure 10. Superposition of the NPC1(NTD)-NPC2 structure with no cholesterol (after 30(+) ns MDs) (white) and the intermediate structure of the NEB-calculated pathway (image #17, Figure 8). The most important change is noticed in the loops containing Tyr192 (NPC1(NTD)) and Met60 (NPC2), which opens to allow the passing of cholesterol. These two residues seem to be involved in nonbonded interactions, which are kept after the opening. The cholesterol molecule is shown as red sticks.

CONCLUSIONS

We have computationally modeled the NPC1(NTD)-NPC2 system and analyzed its time evolution using molecular dynamics simulations. The simulations revealed a large reorganization in the active site pocket with no cholesterol bound, mainly associated with an inward movement of the helices (helix 3, helix 7, and helix8) in NPC1(NTD), and with the loops involved in the interface in NPC2. Moreover, the MM/GBSA calculations show that the binding of cholesterol to the NPC2 moiety stabilizes the NPC1(NTD)-NPC2 system, through interactions of the cholesterol OH terminal with residues of NPC1(NTD). This effect is reversed when the hydroxyl end of cholesterol is buried in the NPC1(NTD) pocket, as the lipophilic interactions in the interface are debilitated by the interaction of cholesterol itself with the residues involved in those interactions. Mutations of key residues of the interface favor the reorganization of the interface to a less stable structure, occurring more easily in the weakened NPC1(NTD)/cholesterol-NPC2 system, as demonstrated by the MD simulations. The model obtained from the calculations is in good agreement with the experimentally available alanine scan results in that it correctly identifies the residues involved in the cholesterol binding and protein−protein association.

The model for cholesterol transport that emerges from the calculations is in general agreement with the one proposed by Brown and Goldstein[10] that rationalizes the egress of cholesterol from endosomes but significantly expands our understanding of the cholesterol transport process at the atomistic level. On the basis of the results of the MM/GBSA and NEB calculations, cholesterol is bound to NPC2, which increases the association constant for the formation of the NPC1(NTD)-NPC2 complex. Once the complex is formed, cholesterol is transferred from NPC2 to NPC1(NTD), leading to a structure that presumably resembles image #14 in Figure 9c where the cholesterol interacts with Thr112 in NPC1-(NTD) and Tyr192, Leu175, and Leu176. This transfer proceeds through the displacement of helices 3, 7, and 8 as well as the adjacent loop, followed by the actual transfer of cholesterol through the opened channel. The transfer of the cholesterol to NPC1(NTD) causes a decrease of the association constant of the protein−protein complex, facilitating the dissociation of the complex. The free NPC2 protein re-enters the cycle, whereas NPC1 transports cholesterol through the membrane by a process not investigated here.

ASSOCIATED CONTENT

Supporting Information

Snapshots of the structures and rmsd from the simulation as well as pdb files for the simulation end points. This material is available free of charge via the Internet at http://pubs.acs.org.

AUTHOR INFORMATION

Corresponding Author

*Phone: 574-631-5876. E-mail: owiest@nd.edu.

Funding

We acknowledge support of this research by the Center for Rare and Neglected Diseases (CRND) at the University of Notre Dame and the Shenzhen Peacock Program (KQTD201103). This work used the Extreme Science and Engineering Discovery Environment (XSEDE), which is supported by National Science Foundation grant number (TG-CHE090124 and CHE120050) and the Center for Research Computing. N.K. gratefully acknowledges support from the Herman Miller and Beulah Pearce Miller Faculty Development, Runkle Faculty Development, and Mildred M. Hoover grants

Notes

The authors declare no competing financial interest.
Pymol sessions with all structures discussed are available from the authors upon request.

ACKNOWLEDGMENTS

We are grateful to Hyock Kwon and Massoud Motamed from the groups of J. L. Goldstein and M. S. Brown at UT Southwestern Medical Center for the coordinates of the initial rigid-body model of NTD-NPC1(NTD)/NPC2.

REFERENCES

(1) Brown, M. S., and Goldstein, J. L. (1986) A receptor-mediated pathway for cholesterol homeostasis. *Science 232*, 34−47.
(2) Brown, M. S., and Goldstein, J. L. (1997) The SREBP pathway: regulation of cholesterol metabolism by proteolysis of a membrane-bound transcription factor. *Cell 89*, 331−340.
(3) King, G., and Sharom, F. J. (2012) Proteins that bind and move lipids: MsbA and NPC1. *Crit. Rev. Biochem. Mol. Biol. 47*, 75−95.
(4) Subramanian, K., and Balch, W. E. (2008) NPC1/NPC2 function as a tag team duo to mobilize cholesterol. *Proc. Natl. Acad. Sci. U.S.A. 105*, 15223−15224.
(5) Rosenbaum, A. I., and Maxfield, F. R. (2011) Niemann-Pick type C disease:molecular mechanisms and potential therapeutic approaches. *J. Neurochem. 116*, 789−795.
(6) Mesmin, B., and Maxfield, F. R. (2009) Intracellular sterol dynamics. *Biochim. Biophys. Acta 1791*, 636−645.
(7) Xu, S., Gu, L., Benoff, B., and Stock, A. M. (2007) Structural basis of sterol binding by NPC2, a lysosomal protein deficient in Niemann-Pick type C2 disease. *J. Biol. Chem. 282*, 23525−23531.
(8) Friedland, N. L., H., L., Lobel, P., and Stock, A. M. (2003) Structure of a cholesterol-binding protein deficient in Niemann-Pick type C2 disease. *Proc. Natl. Acad. Sci. U.S.A. 100*, 2512−2517.
(9) Davies, J. P., and Ioannou, Y. A. (2000) Topological analysis of Niemann-Pick C1 protein reveals that the membrane orientation of the putative sterolsensing domain is identical to those of 3-hydroxy-3-

methylglutaryl-CoA reductase and sterol regulatory element binding protein cleavage-activating protein. *J. Biol. Chem. 275*, 24367−24374.
(10) Kwon, H. J., Abi-Mosleh, L., Wang, M. L., Deisenhofer, J., Goldstein, J. L., Brown, M. S., and Infante, R. E. (2009) Structure of N-terminal domain of NPC1 reveals distinct subdomains for binding and transfer of cholesterol. *Cell 137*, 1213−1224.
(11) Kwon, H. J., Palnitkar, M., and Deisenhofer, J. (2011) The structure of the NPC1L1 N-terminal domain in a closed conformation. *PLoS One 6*, e18722.
(12) Infante, R. E., Wang, M. L., Radhakrishnan, A., Kwon, H. J., Brown, M. S., and Goldstein, J. L. (2008) NPC2 facilitates bidirectional transfer of cholesterol between NPC1 and lipid bilayers, a step in cholesterol egress from lysosomes. *Proc. Natl. Acad. Sci. U.S.A. 105*, 15287−15292.
(13) Xie, X., Brown, M. S., Shelton, J. M., Richardson, J. A., Goldstein, J. L., and Lianga, G. (2011) Amino acid substitution in NPC1 that abolishes cholesterol binding reproduces phenotype of complete NPC1 deficiency in mice. *Proc. Natl. Acad. Sci. U.S.A 108*, 15333−15335.
(14) Wang, M. L., Motamed, M., Infante, R. E., Abi-Mosleh, L., Kwon, H. J., Brown, M. S., and Goldstein, J. L. (2010) Identification of surface residues on Niemann-Pick C2 essential for hydrophobic handoff of cholesterol to NPC1 in lysosomes. *Cell Metab. 12*, 166−173.
(15) Deffieu, M. S., and Pfeffer, S. R. (2011) Niemann-Pick type C 1 function requires lumenal domain residues that mediate cholesterol-dependent NPC2 binding. *Proc. Natl. Acad. Sci. U.S.A. 108*, 18932−18936.
(16) Vance, J. E., and Peake, K. B. (2011) Function of the Niemann-Pick type C proteins and their bypass by cyclodextrin. *Curr. Opin. Lipidol. 22*, 204−209.
(17) Kruth, H. S., Comly, M., Butler, J. D., Vanier, M. T., Fink, J. K., Wenger, D. A., Patel, S., and Pentchev, P. G. (1986) Type C Niemann-Pick disease. Abnormal metabolism of low density lipoprotein in homozygous and heterozygous fibroblasts. *J. Biol. Chem. 261*, 9290−9298.
(18) Pentchev, P. G., Kruth, H. S., Comly, M., Butler, J. D., Vanier, M. T., Wenger, D. A., and Patel, S. (1986) Type C Niemann-Pick disease. A parallel loss of regulatory responses in both the uptake and esterification of low density lipoprotein-derived cholesterol in cultured fibroblasts. *J. Biol. Chem. 261*, 16775−16780.
(19) Vanier, M. (2010) Niemann-Pick disease type C. *Orphanet J. Rare Dis. 5*, 16.
(20) Munkacsi, A. B., Chen, F. W., Brinkman, M. A., Higaki, K., Gutiérrez, G. D., Chaudhari, J., Layer, J. V., Tong, A., Bard, M., Boone, C., Ioannou, Y. A., and Sturley, S. L. (2011) An "exacerbate-reverse" strategy in yeast identifies histone deacetylase inhibition as a correction for cholesterol and sphingolipid transport defects in human Niemann-Pick type C disease. *J. Biol. Chem. 286*, 23842−23851.
(21) Helquist, P., and Wiest, O. (2009) Current status of drug therapy development for Niemann Pick type C disease. *Drugs Future 34*, 315−331.
(22) Peake, K. B., and Vance, J. E. (2012) Normalization of cholesterol homeostasis by 2-hydroxypropyl-β-cyclodextrin in neurons and glia from Niemann-Pick C1 (NPC1)-deficient mice. *J. Biol. Chem. 287*, 9290−9298.
(23) Pipalia, N. H., Cosner, K. C., Huang, A., Chatterjee, A., Bourbon, P., Farley, N., Helquist, P., Wiest, O., and Maxfield, F. R. (2011) Histone deacetylase inhibitor treatment dramatically reduces cholesterol accumulation in Niemann-Pick type C1 mutant human fibroblasts. *Proc. Natl. Acad. Sci. U.S.A. 108*, 5620−5625.
(24) te Vruchte, D., Lloyd-Evans, E., Veldman, R. J., Neville, D. C. A., Dwek, R. A., Platt, F., van Blitterswijk, W. J., and Sillence, D. J. (2004) Accumulation of glycosphingolipids in Niemann-Pick C disease disrupts endosomal transport. *J. Biol. Chem. 279*, 26167−26175.
(25) Chang, T.-Y., Reid, P. C., Sugii, S., Ohgami, N., Cruz, J. C., and Chang, C. C. (2005) Niemann-Pick type C disease and intracellular cholesterol trafficking. *J. Biol. Chem. 290*, 20917−20920.
(26) Moles, A., Tarrats, N., Fernández-Checa, J. C., and Mar, M. (2011) Cathepsin B overexpression due to acid sphingomyelinase ablation promotes liver fibrosis in Niemann-Pick disease. *J. Biol. Chem. 287*, 1178−1188.
(27) Carette, J. E., Raaben, M., Wong, A. C., Herbert, A. S., Obernosterer, G., Mulherkar, N., Kuehne, A. I., Kranzusch, P. J., Griffin, A. M., Ruthel, G., Dal Cin, P., Dye, J. M., Whelan, S. P., Chandran, K., and Brummelkamp, T. R. (2011) Ebola virus entry requires the cholesterol transporter Niemann−Pick C1. *Nature 477*, 340−343.
(28) Cote, M., Misasi, J., Ren, T., Bruchez, A., Lee, K., Filone, C. M., Hensley, L., Li, Q., Ory, D., Chandran, K., and Cunningham, J. (2011) Small molecule inhibitors reveal Niemann−Pick C1 is essential for Ebola virus infection. *Nature 477*, 344−348.
(29) Jorgensen, W. L., Chandrasekhar, J., Madura, J. D., Impey, R. W., and Klein, M. L. (1983) Comparison of simple potential functions for simulating liquid water. *J. Chem. Phys. 79*, 926−935.
(30) Case, D. A., Darden, T. A., Cheatham, T. E., Simmerling, C. L., Wang, J., Duke, R. E., Luo, R., Walker, R. C., Zhang, W., Merz, K. M., Roberts, B., Wang, B., Hayik, S., Roitberg, A., Seabra, G., Kolossváry, I., Wong, K. F., Paesani, F., Vanicek, J., Liu, J., Wu, X., Brozell, S. R., Steinbrecher, T., Gohlke, H., Cai, Q., Ye, X., Wang, J., Hsieh, M., Cui, G., Roe, D. R., Mathews, D. H., Seetin, M. G., Sagui, C., Babin, V., Luchko, T., Gusarov, S., Kovalenko, A., and Kollman, P. A. (2010) *AMBER11*, University of California, San Francisco, CA.
(31) Wang, J., Wang, W., Kollman, P. A., and Case, D. A. (2006) Automatic atom type and bond type perception in molecular mechanical calculations. *J. Mol. Graphics Modell. 25*, 247−260.
(32) Wang, J., Wolf, R. M., Caldwell, J. M., Kollman, P. A., and Case, D. A. (2004) Development and testing of a general Amber force field. *J. Comput. Chem. 25*, 1157−1174.
(33) Bayly, C. I., Cieplak, P., Cornell, W. D., and Kollman, P. A. (1993) A well-behaved electrostatic potential based method using charge restraints for determining atom-centered charges: the RESP model. *J. Phys. Chem. 97*, 10269−10280.
(34) Fox, T., and Kollman, P. A. (1998) Application of the RESP methodology in the parametrization of organic solvents. *J. Phys. Chem. B 102*, 8070−8079.
(35) Ryckaert, J. P., Ciccotti, G., and Berendsen, H. J. C. (1977) Numerical integration of the cartesian equations of motion of a system with constraints: molecular dynamics of n-alkanes. *J. Comput. Phys. 23*, 327−341.
(36) Pastor, R. W., Brooks, B. R., and Szabo, A. (1988) An analysis of the accuracy of Langevin and molecular dynamics algorithms. *Mol. Phys. 65*, 1409−1419.
(37) Essmann, U., Perera, L., Berkowitz, M. L., Darden, T., Lee, H., and Pedersen, L. G. (1995) A smooth particle mesh Ewald method. *J. Chem. Phys. 103*, 8577−8593.
(38) Petersen, H. G. (1995) Accuracy and efficiency of the particle-mesh-ewald method. *J. Chem. Phys. 103*, 3668−3679.
(39) Hou, T., Wang, J., Li, Y., and W., W. (2011) Assessing the performance of the MM/PBSA and MM/GBSA methods. 1. The accuracy of binding free energy calculations based on molecular dynamics simulations. *J. Chem. Inf. Mod. 51*, 69−82.
(40) Wang, J., Hou, T., and Xu, X. (2006) Recent advances in free energy calculations with a combination of molecular mechanics and continuum models. *Cur. Comput.-Aided Drug Des. 2006*, 95−103.
(41) Kollman, P. A., Massova, I., Reyes, C., Kuhn, B., Huo, S., Chong, L., Lee, M., Lee, T., Duan, Y., Wang, W., Donini, O., Cieplak, P., Srinivasan, J., Case, D. A., and Cheatham, T. E. (2000) Calculating structures and free energies of complex molecules: combining molecular mechanics and continuum models. *Acc. Chem. Res. 33*, 889−897.
(42) Zoete, V., and Michielin, O. (2007) Comparison between computational alanine scanning and per-residue binding free energy decomposition for protein-protein association using MM-GBSA: application to the TCR-p-MHC complex. *Proteins 67*, 1026−1047.
(43) Li, T., Froeyen, M., and Herdewijn, P. (2008) Computational alanine scanning and free energy decomposition for E. coli type I

signal peptidase with lipopeptide inhibitor complex. *J. Mol. Graphics Modell. 26*, 813−823.
(44) Massova, I., and Kollman, P. A. (1999) Computational alanine scanning to probe protein−protein interactions: a novel approach to evaluate binding free energies. *J. Am. Chem. Soc. 121*, 8133−8143.
(45) Zoete, V., Irving, M. B., and Michielin, O. (2010) MM-GBSA binding free energy decomposition and T cell receptor engineering. *J. Mol. Recognit. 23*, 142−152.
(46) Gohlke, H., Kiel, C., and Case, D. A. (2003) Insights into protein−protein binding by binding free energy calculation and free energy decomposition for the Ras−Raf and Ras−RalGDS complexes. *J. Mol. Biol. 330*, 891−913.
(47) Mathews, D. H., and Case, D. A. (2006) Nudged elastic band calculation of minimal energy paths for the conformational change of a GG non-canonical pair. *J. Mol. Biol. 357*, 1683−1693.
(48) Tsui, V., and Case, D. A. (2001) Theory and applications of the generalized Born solvation model in macromolecular simulations. *Biopolymers 56*, 275−291.
(49) Tsui, V., and Case, D. A. (2000) Molecular dynamics simulations of nucleic acids with a generalized born solvation model. *J. Am. Chem. Soc. 122*, 2489−2498.
(50) Shen, Y., Liu, J., Estiu, G., Isin, B., Lee, D.-S., Barabási, A.-L., Kapatral, V., Wiest, O., and Oltvai, Z. N. (2009) A blueprint for antimicrobial hit discovery targeting metabolic networks. *Proc. Natl. Acad. Sci. U.S.A. 106*, 1082−1087.
(51) Van Nostrand, K. P., Kennedy, S. D., Turner, D. H., and Mathews, D. H. (2011) Molecular mechanics investigation of an adenine adenine non-canonical pair conformational change. *J. Chem. Theory Comput. 7*, 3779−3792.
(52) Reblova, K., Strelcova, Z., Kulhanek, P., Besseova, I., Mathews, D. H., Van Nostrand, K. P., YiIildirim, Y., Turner, D. H., and Sponer, J. (2010) An RNA molecular switch: intrinsic flexibility of 23S rRNA helices 40 and 68 5′-UAA/5′-GAN internal loops studied by molecular dynamics methods. *J. Chem. Theory Comput. 6*, 910−929.